

Article

Surface Modification of PVDF and PTFE Hollow Fiber Membranes for Enhanced Nitrogen Removal in a Membrane-Aerated Biofilm Reactor

Wenfeng Zai ^{1,2}, Yangman Chen ^{2,3}, Qingdong Qin ³, Xiangkun Li ¹ and Dezhao Liu ^{2,4,*} 

¹ School of Civil and Transportation Engineering, Hebei University of Technology, Tianjin 300401, China; 202231604008@stu.hebut.edu.cn (W.Z.); xkli312@163.com (X.L.)

² Institute of Agri-Biological Environment Engineering, College of Biosystems Engineering and Food Science, Zhejiang University, Hangzhou 310058, China; 220204956@seu.edu.cn

³ School of Civil Engineering, Southeast University, Nanjing 211189, China; qinqingdong@seu.edu.cn

⁴ Key Laboratory of Equipment and Informatization in Environment Controlled Agriculture from Ministry of Agriculture and Rural Affairs of China, Key Laboratory of Intelligent Equipment and Robotics for Agriculture of Zhejiang Province, Hangzhou 310058, China

* Correspondence: dezhaoliu@zju.edu.cn

Highlights:

- Plasma-grafting acrylic acid composite membrane for MABR was prepared.
- Higher O₂ transfer rate and better hydrophilicity for modified membranes than pristine.
- Modified PVDF membrane demonstrated superior nitrogen removal during startup.
- Activity of denitrifying bacteria was enhanced in the modified PVDF MABR.

Abstract: Microporous membranes such as polytetrafluoroethylene (PTFE) and polyvinylidene fluoride (PVDF) often exhibit suboptimal hydrophilicity and microbial adhesion, which impede effective nitrogen removal in membrane-aerated biofilm reactors (MABRs), particularly during initial operational phases. To address this issue, the present study introduced acrylic acid (AA) following plasma treatment (P) to enhance membrane performance, thereby engineering a novel composite material optimized for MABR applications. Four MABRs—Reactor with pristine PVDF membrane (R-PVDF), Reactor with composite PVDF membrane (R-PVDF-P-AA), Reactor with pristine PTFE membrane (R-PTFE), and Reactor with composite PTFE membrane (R-PTFE-P-AA)—were evaluated. The modified membranes displayed enhanced roughness and hydrophilicity, which improved biocompatibility and variably increased the oxygen transfer efficiency. Notably, the R-PVDF-P-AA configuration showed a significant enhancement in the removal rates of NH₄⁺-N and total nitrogen (TN), achieving 78.5% and 61.3%, respectively, which was markedly higher than those observed with the original membranes. In contrast, the modified R-PTFE-P-AA exhibited lower removal efficiencies, with NH₄⁺-N and TN reductions of approximately 60.0% and 49.5%. Detailed microbial community analysis revealed that the R-PVDF-P-AA membrane supported robust commensalism between ammonia-oxidizing and denitrifying bacteria, underpinning the improved performance. These findings highlight the critical role of surface chemistry and microbial ecology in optimizing the function of MABRs.

Keywords: membrane-aerated biofilm reactor; plasma modification; nitrogen removal; PVDF; PTFE



Citation: Zai, W.; Chen, Y.; Qin, Q.; Li, X.; Liu, D. Surface Modification of PVDF and PTFE Hollow Fiber Membranes for Enhanced Nitrogen Removal in a Membrane-Aerated Biofilm Reactor. *Water* **2024**, *16*, 1747. <https://doi.org/10.3390/w16121747>

Academic Editor: Constantinos V. Chrysikopoulos

Received: 11 May 2024

Revised: 14 June 2024

Accepted: 18 June 2024

Published: 20 June 2024



Copyright: © 2024 by the authors. Licensee MDPI, Basel, Switzerland. This article is an open access article distributed under the terms and conditions of the Creative Commons Attribution (CC BY) license (<https://creativecommons.org/licenses/by/4.0/>).

1. Introduction

The membrane-aerated biofilm reactor (MABR) has garnered increasing attention due to its high efficiency and low-energy oxygen delivery in wastewater treatment [1,2]. The MABR mechanism involves oxygen diffusion through gas-permeable membranes, promoting biofilm growth on the exterior of the membrane and consequently enhancing the degradation of organic matter in sewage [3,4]. It is noted that the oxygen concentration

gradient plays a crucial role in influencing bacterial growth within biofilms [5]. Specifically, the proximity to the biofilm–membrane interface creates an aerobic zone with low organic substrate, while the region near the biofilm–liquid interface forms an anoxic zone with high organic content. Nitrifying bacteria, such as ammonia-oxidizing bacteria (AOB) and nitrite-oxidizing bacteria (NOB), dominate the aerobic zone, while denitrifying bacteria prevail in the anoxic region [6]. This symbiotic environment within a single MABR enables simultaneous nitrification and denitrification (SND) by fostering a conducive habitat for aerobic and anaerobic microorganisms to remove nitrogen [7].

Considering the performance, selecting an appropriate membrane is critical to the MABR process. Different materials and manufacturing technologies result in diverse morphologies, pore characteristics, and porosity in the membrane surface [8]. Currently, three main types of membrane materials are utilized for MABR operations: dense membranes, hydrophobic microporous membranes, and composite membranes [9,10]. The typical hydrophobic microporous membrane includes PP, PVDF, and PTFE. In comparison to dense and composite membranes, the hydrophobic microporous membrane exhibits higher gas flux and a moderate price [8,11]. However, PVDF also presents apparent drawbacks. Owing to poor hydrophilicity on the outer surface, gas transfer through the pores may destroy the biofilm attached to the membrane surfaces. Additionally, PTFE has poor bonding performance and microbial compatibility, making it challenging for microorganisms to adhere. Consequently, an increasing number of researchers are employing surface modification techniques to develop composite membranes with improved microbial affinity on the surface of MABR membrane materials. Coating membranes with L-3,4-dihydroxyphenylalanine has been demonstrated to effectively increase the PVDF membrane surface roughness and enhance bacterial attachment [12]. Likewise, surface decorating of the PVDF membrane with hydrophobic Polyether-block-polyamide copolymer 2533 was also more conducive to microorganism adhesion [13]. Nonetheless, such coating can only temporarily improve the properties of the membrane surface as the surface layer is prone to degradation during storage or use.

Plasma-induced polymerization has been successfully used to modify membrane surfaces [14,15]. A simple treatment with inert gas, nitrogen, or oxygen, followed by air exposure, can generate peroxides that serve as reactive sites for subsequent monomer grafting and polymerization [16]. This method allows plasma to alter the physical and chemical properties of polymeric surfaces while preserving the bulk property of the membrane. Moreover, the entire process conserves energy, requires a short treatment time, and offers high efficiency and uniformity of material surface treatment compared to other traditional methods. Acrylic acid (AA) has found widespread application in surface modification with the introduction of many carboxyl groups. For instance, it has been applied to bind chitosan for superior biocompatibility in biomedical engineering [17,18]. Low-pressure air plasma treatment induces AA graft polymerization, forming a dense layer of a polyacrylic acid graft that significantly improves hydrophilicity, reducing the contact angle from 57.62° to 29.26° [19]. Additionally, in a study by Khongnakorn [20], plasma-grafting polymerization of AA monomers was observed to increase surface roughness and hydrophilicity. Based on the solid hydrophilicity and good biocompatibility of AA, the membrane modified by the self-polymerization of AA may exhibit excellent performance in MABRs. However, the application of plasma-grafting AA monomers to modify membranes in MABR systems has yet to be investigated.

Therefore, in this experiment, plasma treatment was utilized to initiate liquid-phase grafting polymerization of acrylic acid, aiming to enhance the hydrophilicity of PVDF and PTFE membranes for their application in MABRs and boost biological affinity ability. The objectives are to (i) compare the morphology, structures, contact angle, and oxygen mass transfer capability of the modified membrane modules with those of the control, (ii) assess the nitrogen removal performance of each MABR device in startup phase, and (iii) understand how microorganisms organize a stable community structure on the modified membranes to enhance performance.

2. Materials and Methods

2.1. Membrane Modification and Characterization

The pristine PVDF hollow fiber membrane and PTFE hollow fiber membrane, with pore sizes of 0.05 μm and 0.1–0.4 μm , were acquired from Jiangxi Enhao Environmental Protection Co., Ltd. (Jiangxi, China). Acrylic acid, sodium sulfite, and cobalt chloride were obtained from Aladdin Company, while argon was procured from Nanjing Special Gas Co., Ltd. (Nanjing, China). The specific modification process is detailed below: The original membranes were initially cleaned using an ethanol solution and deionized water in an ultrasonic cleaner to remove impurities, followed by air-drying at room temperature for later use. Subsequently, under vacuum conditions, argon gas was introduced at a controlled flow rate ranging between 100 and 120 mL/min, and plasma treatment using PT-5S (Sanheoda, Shenzhen, China) was conducted. The PVDF membrane was subjected to 30 W power for 80 s, while the PTFE membrane received 70 W power for the same duration. Subsequently, both were exposed to ambient air for 10 min, as determined through preliminary experiment. Following this, the plasma-treated membrane materials were immersed in a 20 wt% aqueous acrylic acid solution at 50 °C for varying coating times. After that, the modified membranes were meticulously washed with deionized water five times and then placed for drying. There are four distinct membrane types after surface modification of hollow fiber membranes, including pristine PVDF, modified PVDF with plasma graft acrylic acid, pristine PTFE, and modified PTFE with acrylic acid, referred to as PVDF, PVDF-P-AA, PTFE, and PTFE-P-AA, respectively.

The surface morphologies of membranes were observed by scanning electron microscopy (GeminiSEM300, Carl Zeiss, Oberkochen, Germany). The functional groups present on the membrane surface were analyzed via Fourier transform infrared spectroscopy (NicoLET iS50, Thermo Fisher, Waltham, USA). Additionally, the contact angles of the membranes were measured using water as the detection liquid on a contact angle meter (Dataphysics, DCA20, Filderstadt, Germany). The oxygen transfer rate (OTR) indicates the oxygenation capacity of the membrane in MABR systems. Moreover, the OTR was measured as follows: (i) the membrane module was immersed in a beaker containing 0.5 L of deionized water, to which sodium sulfite and cobalt chloride were added to eliminate dissolved oxygen; (ii) the aeration pump was turned on to adjust the different aeration pressures (10 kpa, 15 kpa, 20 kpa), and the concentration of dissolved oxygen (DO) at different times was recorded; and (iii) calculations were performed according to the following OTR equation.

$$\text{OTR} = \text{KLa} \times V \times C_s$$

where KLa = oxygen transfer coefficient (min^{-1}), C_s = dissolved oxygen concentration (mg/L) in equilibrium with gas as given Henry's law, and V = liquid volume (L) during dissolved oxygen testing.

2.2. MABR Configuration and Operating Condition

Figure 1 illustrates the schematic of the MABR system. Four identical MABRs were established, each with an actual working volume of 1.88 L (a cylinder 10 cm in diameter and 25 cm in height) to assess disparities between the aforementioned membranes (PVDF, PVDF-P-AA, PTFE, and PTFE-P-AA). Twenty-six pieces of hollow fibers, each with an available length of 300 mm, were installed into the four reactors, resulting in a filling density of 22.9 m^2/m^3 of membrane, designated as R-PVDF, R-PVDF-P-AA, R-PTFE, and R-PTFE-P-AA, respectively. Wastewater was continuously supplied using a peristaltic pump, and the effluent was discharged through an overflow. The reactor was designed with an inlet and an outlet for water circulation, with a circulation pump controlling the flow rate. Air was supplied into the membrane lumen using an air pump, while the exhaust gas remained closed. Periodically, the upper outlet of the reactor was opened to exhaust waste gas. The experimental temperature was maintained at 25 ± 0.5 °C, and the pH was kept between 7.0 and 8.0.

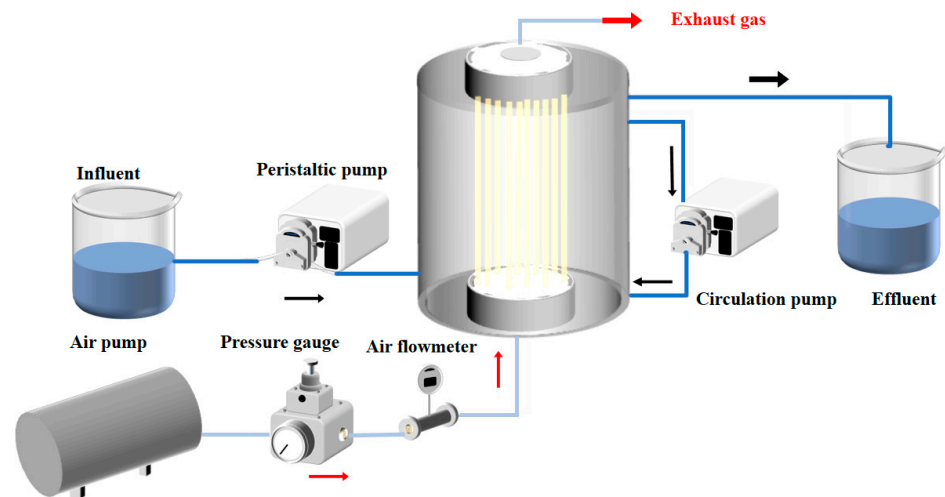


Figure 1. Schematic diagram of the MABR. (1) The red arrow represents the direction of gas flow. (2) The black arrow represents the direction of wastewater.

The biofilm formation process commenced by applying the method of inoculating activated sludge. Approximately 0.3 L of activated sludge with a mixed liquor suspended solids (MLSS) value of 5000 mg/L was introduced into the reactor filled with experimental water with a 100 mL/min flow rate for aeration. After circulating for seven days, the inoculated sludge was discharged from the reactor to start the operation stages. Synthetic wastewater was used to simulate actual low carbon/nitrogen ratio domestic wastewater, in which $C_6H_{12}O_6$ (150 mg/L) was used as a carbon source; NH_4Cl (123 mg/L) and KH_2PO_4 (30 mg/L) were added as nitrogen and phosphorus elements to maintain microbial growth. The remaining components of the synthetic wastewater included Na_2CO_3 100 mg/L, $NaHCO_3$ 50 mg/L, $MgSO_4 \cdot 7H_2O$ 55 mg/L, $CuSO_4 \cdot 5H_2O$ 2 mg/L, $MnCl_4 \cdot H_2O$ 2 mg/L, $NiCl \cdot H_2O$ 2 mg/L, $CoCl_2 \cdot 6H_2O$ 2 mg/L, and H_3BO_4 2 mg/L and $ZnSO_4$ 0.1 mg/L.

2.3. Analytical Methods

During the experiment, Ammonium ($NH_4^+ - N$), nitrite ($NO_2^- - N$), and nitrate ($NO_3^- - N$) of the effluent turbidity were measured by a Multiparameter Spectrophotometer (Cary 60 UV-VIS, Agilent Technologies, America) following standard methods. The DO and pH levels were measured using a portable dissolved oxygen meter (JPB-607A, Leici Instrument Factory, Shanghai, China) and a pH meter (ST-3100, Ohus Instruments, Changzhou, China), respectively.

To investigate the alteration of microbial community structure within the biofilm in response to membrane surface structure during the initial startup period, the inoculation sludge and biofilm samples obtained from the membrane surface of MABRs at different time points (on Day 20 and 30) were preserved at $-80^\circ C$ until analysis. DNA extraction and PCR amplification of biomass samples were conducted following standard protocols. Subsequently, Illumina sequencing was employed, and rigorous quality control measures were implemented to ensure the reliability of the obtained sequence data. This comprehensive approach was designed to elucidate microbial community structure, diversity, and species abundance alterations.

3. Results and Discussion

3.1. Performance and Characterization of Modified Membrane Fibers

3.1.1. Surface Hydrophilicity of Modified Hollow Fiber Membranes

Contact angle measurement is one of the simplest methods for determining the hydrophobic or hydrophilic of the outer surface. The application of plasma technology to treat the membrane surface introduces diverse functional groups and modifies its hydrophilic properties. With the increase in these functional groups, the surface wettability demon-

strates a substantial enhancement [21], thus benefiting biofilm growth and the microbial domestication period reduction [22]. As expected, the contact angle of the PVDF membrane was found to decrease to 78.5° after plasma-assisted acrylic grafted treatment, as shown in Figure 2a. This happened because of the graft polymerization reaction of acrylic acid on the active site after plasma treatment, which gradually formed a dense layer of poly acrylic acid on the modified membrane surface, improving the hydrophilicity of the PVDF-P-AA membrane [23]. It is noteworthy that continuous soaking for over 50 min does not further augment hydrophilicity. The PTFE-P-AA membrane exhibited optimal hydrophilicity (89.8°) with a 30 min soaking time, as depicted in Figure 2b. In contrast to the PVDF membrane, the contact angle of the modified PTFE membrane consistently increased with extended soaking time, potentially due to the structure of the PTFE causing the thin polyacrylic layer to detach within such a confined region. Notably, the contact angle of the PTFE-P-AA membrane exhibited minimal change (approaching 90°) when the soaking time exceeded 120 min, possibly indicating the contribution of graft stability or even a decrease due to the rapid consumption of monomers through homopolymerization [14].

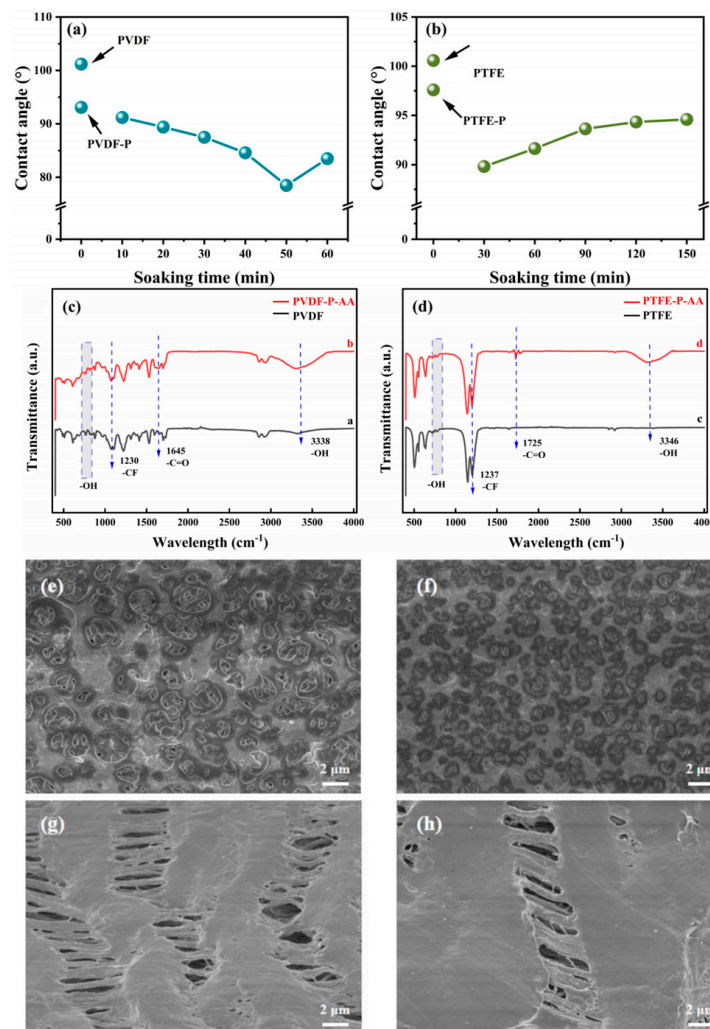


Figure 2. Surface characterization of the membranes: The contact angles of plasma grafted acrylic acid PVDF (a) and PTFE (b) with soaking time. FTIR spectra of the pristine and modified membranes PVDF (c) and PTFE (d). SEM ($\times 3000$) images of PVDF pristine membrane (e), PVDF-P-AA membrane (f), PTFE pristine membrane (g), and PTFE modified membrane (h).

3.1.2. Surface Chemistry of Modified Hollow Fiber Membranes

FT-IR technology was applied to detect the material surface to verify whether the membrane successfully grafted functional groups [24]. It is clear from Figure 2c,d that all samples showing C-F stretching vibration peaks at 1000–1300 cm^{-1} belong to the fundamental bonds the membrane material possesses. The out-of-plane bending vibration peak of the hydroxyl group (-OH) is typically located within the wavenumber range of 700 to 800 cm^{-1} , but it was not evident in this study. However, the new absorption bands of PVDF-P-AA and PTFE-P-AA modified membranes exhibited stretching vibrations representing -OH at 3000–3700 cm^{-1} . Moreover, a pronounced enhancement of the -C=O stretching vibration peak (1600–1800 cm^{-1}) of the modified membranes was also observed, especially PVDF-P-AA, illustrating that carboxyl groups were grafted onto the material surface. Acrylic acid was successfully “locked in” the membrane surface after plasma treatment, as shown by the FT-IR result. -OH and -C=O, as valuable functional groups that can affect the hydrophilicity of the material surface, may play a positive role in the application of MABR.

3.1.3. Morphology of Membrane Surface

The SEM images of the original membranes and modified composite membranes are shown in Figure 2e–h. The pore-like structure of the PVDF-based membrane was distributed in a dotted pattern. Notably, compared to the original membrane, dense and tiny pores emerged on the surface of the PVDF-P-AA membrane. In addition, the edge of the pores after modification was irregular and rough, providing a suitable environment for the subsequent attachment and growth of microorganisms. Such a situation may be attributed to the etching effect caused by high-energy plasma particles colliding [25]. However, the pore size clearly varied, and a small aperture area may have been clogged in subsequent applications, significantly reducing the membrane utilization efficiency. The shapes of microporous PTFE and PTFE-P-AA membranes are displayed with banded cavities, thin and long, as shown in Figure 2g,h. The pristine PTFE membrane was cruder on the surface of the membrane material, while most of the PTFE-P-AA membrane surfaces were neat. Nevertheless, the pore distribution of PTFE-P-AA was even more consistent in size. This structural distribution can provide a more uniform oxygen gradient in follow-up applications.

Overall, using plasma-induced acrylic acid liquid-phase grafting polymerization to treat microporous aeration membranes can achieve the goal of changing their surface structures. Whether the changes in various properties of the membrane surface are ultimately beneficial for microbial biofilm formation and improving its treatment efficiency needs to be verified by MABR.

3.1.4. Oxygen Supply Capacity of Membranes

The mass transfer efficiency of various membrane modules was assessed by measuring the DO concentration in the aqueous solution over a specific duration at a uniform pressure (Figure 3). In a gas dispersion process facilitated by a porous membrane, gas dispersion into bubbles occurs only after overcoming the resistance generated by the membrane pores [26]. Even though a dense layer of poly acrylic acid on the surface was formed after modification, the OTR of the PVDF-P-AA membrane was 0.22 $\text{mg O}_2 \cdot \text{min}^{-1}$, still higher by 46.7% compared to the pristine PVDF (0.15 $\text{mg O}_2 \cdot \text{min}^{-1}$), which may be due to the main poly acrylic acid layer distributed in the membrane surface instead of pores areas. Differing from the PVDF-P-AA modified membrane, the oxygen transfer capacity of the PTFE-P-AA membrane was lower than that of the pristine PTFE membrane at the beginning of the test, and then it increased. At optimal aeration pressure (20 kpa), the OTR of PTFE and PTFE-P-AA membranes was 0.21 $\text{mg O}_2 \cdot \text{min}^{-1}$ and 0.26 $\text{mg O}_2 \cdot \text{min}^{-1}$ after approximately 60 min. The OTR of the two types of modified membranes by plasma-grafting AA monomers improved in some ways, indicating that membrane assembly should be able to provide supply of air for MABRs to treat pollutants. However, it should be pointed out that PVDF-

P-AA (46.7%) displayed a higher enhancement than PTFE-P-AA (23.8%), providing more channels for oxygen mass transfer in later MABR applications.

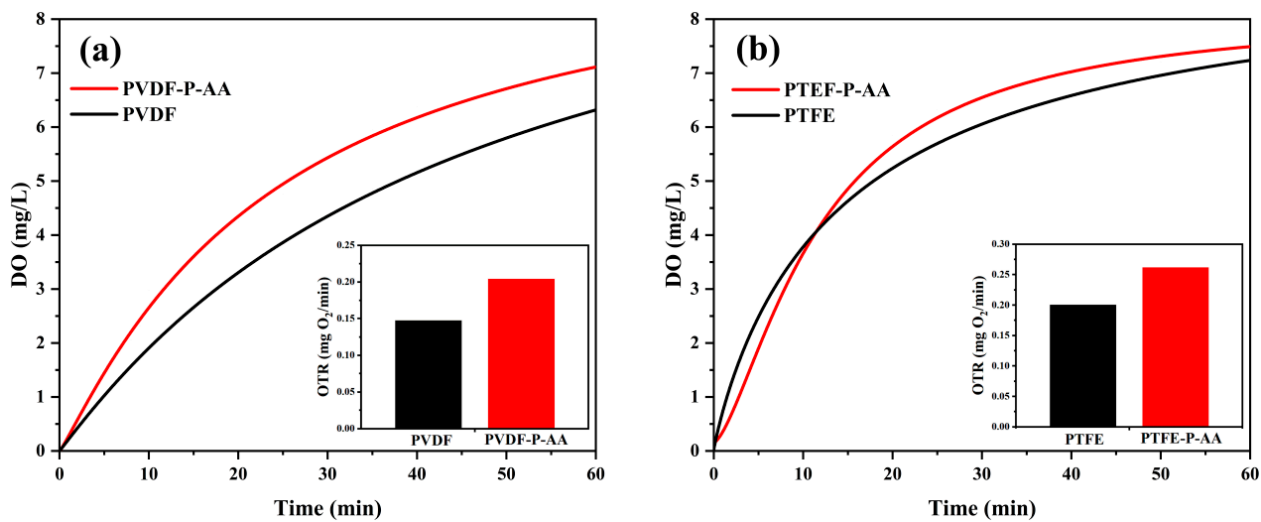


Figure 3. Oxygen transfer test of the membranes: (a) pristine PVDF and PVDF-P-AA membranes and (b) pristine PTFE and PTFE-P-AA membranes.

3.2. Performance of MABRs during the Startup Phase

3.2.1. PVDF and PVDF-P-AA Reactors

The performance of the startup period in MABRs regarding nitrogen removal efficiencies was evaluated and presented in the following figure (Figure 4). Initially, the $\text{NH}_4^+\text{-N}$ removal rate of R-PVDF-P-AA was approximately 26.8%, whereas R-PVDF (Figure 4a) only maintained a rate below 10%. A significant improvement was observed in R-PVDF-P-AA as the operation progressed, reaching 61.2%. A better hydrophilicity and DO transport ability of the PVDF-modified membrane benefit microorganisms [27]. AOB and NOB, as aerobic bacteria, tend to aggregate within the inner part of the modified fiber membrane, where there is a more abundant concentration of DO. A suitable oxygen environment enhanced the biofilm formation of the device, which is beneficial for converting $\text{NH}_4^+\text{-N}$ into $\text{NO}_2^-\text{-N}$ and $\text{NO}_3^-\text{-N}$. Regarding $\text{NH}_4^+\text{-N}$ removal (about 78.5%) in the late startup phase, R-PVDF-P-AA demonstrated a better nitrification efficiency at the same aeration pressure.

In terms of the TN removal rate, as depicted in Figure 4c, R-PVDF-P-AA reached its peak (59.4%) after approximately 18 days of operation. It is conceivable that nitrifying and denitrifying bacteria systematically established a framework for synchronous nitrification and denitrification during this specific period. Conversely, the TN removal rate in R-PVDF was relatively deficient, likely due to the limited attraction of microorganisms, with only a sparse presence of denitrifying bacteria on the material surface. Wang et al. compared the wastewater treatment effects of modified and original membranes under identical conditions during the biofilm formation process and found that the modified membrane surface expedited the formation of a denser biofilm more efficiently [15]. After 26 days of operation, the TN removal rate stabilized, with an average removal rate of 61.3% in R-PVDF-P-AA, indicating a superior capacity for degrading nitrogen pollutants. As continued, there was no significant improvement in the TN removal rate, which could be attributed to the thin biofilms formed during the startup phase, transferring excess oxygen to the bulk liquid, thereby favoring nitrification by nitrifying bacteria.

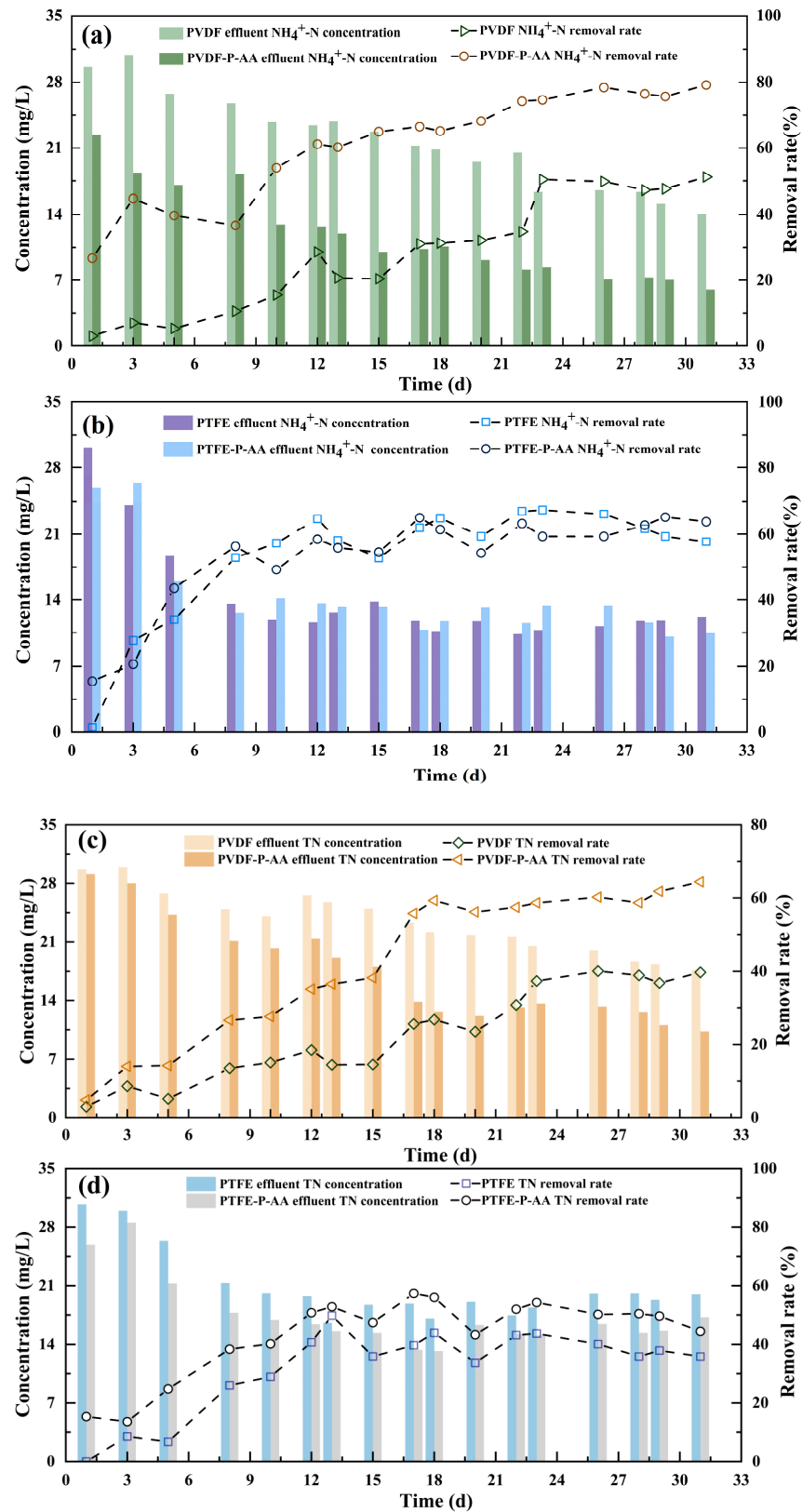


Figure 4. Concentration and removal rate of $\text{NH}_4^+\text{-N}$ and TN during MABRs startup: (a) PVDF and PVDF-P-AA effluent $\text{NH}_4^+\text{-N}$ and removal rate; (b) PTFE and PTFE-P-AA effluent $\text{NH}_4^+\text{-N}$ and removal rate; (c) PVDF and PVDF-P-AA effluent TN and removal rate; (d) PTFE and PTFE-P-AA effluent TN and removal rate.

3.2.2. PTFE and PTFE-P-AA Reactors

The NH_4^+ -N removal effect of R-PTFE and R-PTFE-P-AA is depicted in Figure 4b. Both continued to display an increasing rate in the early period of membrane formation. By the 10th day, the removal rates of R-PTFE and R-PTFE-P-AA were recorded at 57.2% and 49.2%, respectively. At this juncture, microorganisms mainly relied on gravity and weak polarity to adhere to the surface of the membrane material, and the performance of R-PTFE-P-AA did not exhibit significant superiority over that of the R-PTFE. Subsequently, as the operation continued, the effluent of NH_4^+ -N began to stabilize, as observed on the 23rd day, with the removal rate reaching approximately 60%. This stabilization indicated that the adhesion of aerobic nitrifying bacteria to the surface of the membrane material remained consistent, with the removal rate exhibiting no future significant alterations.

During the first 13 days of the reaction, the TN removal rate for each device maintained a stable improving trend, and the reactor gradually accumulated denitrifying bacteria and leveraged its counter-diffusion oxygen supply characteristics to achieve synchronous nitrification and denitrification. Compared to R-PTFE, R-PTFE-P-AA exhibited marginally superior TN removal, achieving a rate of 49.5%, possibly attributable to its improved hydrophilicity, oxygen flux, and other associated parameters. It could simultaneously attract AOB, NOB, and denitrifying bacteria, facilitating their aggregation and biofilm formation. By approximately the 17th day, R-PTFE-P-AA peaked at a 57.39% TN removal rate. However, by the 20th day, the TN load for both sets of devices showed a fluctuating trend. This phenomenon could be attributed to the ongoing water quality adaptation phase, resulting in weak microorganism adhesion and subsequent detachment. The high ability of oxygen transfer may limit the formation of an anaerobic zone on the outer layer of the biofilm and the growth of denitrifying bacteria [8]. Additionally, agitation within the system may have caused microorganisms to dislodge, potentially leading to the detachment of some denitrifying bacteria adhered to the outermost layer of the biofilm, thereby maintaining a high-load TN state.

3.3. Analysis of Microbial Community Diversity and Community Structure

3.3.1. Analysis of Microbial Community Diversity

In order to understand how microorganisms organize a stable community structure on the modified membranes for improved process performance, samples were taken on the 20th and 30th day of the biofilm formation period in each device, and 16S rRNA high-throughput sequencing was performed. The table delineating the respective sample groups and the corresponding time points for different samples is presented in Table 1. Notably, the first numeral denotes the sampling instances, while the second digit signifies the diverse reaction devices utilized in this study.

Table 1. Sample name correspondence table.

Sample ID	Sampling Device	Time (Day)
1-1	R-PVDF	20
1-2	R-PVDF-P-AA	20
1-3	R-PTFE	20
1-4	R-PTFE-P-AA	20
2-1	R-PVDF	30
2-2	R-PVDF-P-AA	30
2-3	R-PTFE	30
2-4	R-PTFE-P-AA	30

The Alpha Diversity Index, as delineated in Table 2, serves as a crucial metric reflecting the abundance and diversity of microbial communities, thus portraying the variations in microbial species richness and community diversity across distinct samples. Notably, the microbial community richness within the samples can be discerned through Operational Taxonomic Units (OTUs) and Chao indices. As evidenced by Table 2, each reactor

demonstrated a discernible increasing trend in microbial abundance with the progression of biofilm formation. The R-PVDF-P-AA had significantly higher OTUs and Chao indices on day 30, signifying an extensive array of species enriching the biofilm and contributing to a more efficient NH_4^+ -N removal rate. Moreover, species abundance in the 2-4 reactor was comparatively lower than in the 2-2 reactor. This disparity can be attributed to the characteristics of the PTFE membrane surface, which elevate the complexity of the bacterial attachment process, consequently influencing community abundance. Notably, the coverage index for all samples in the table surpassed 99%, indicating that the sequencing outcomes accurately portray the microbial composition in each sample. The Shannon index is typically applied as an estimator of microbial diversity, while the Simpson index quantitatively describes the biodiversity of a specific region. By comparing the values of these indices, the diversity of each community in the sample can be elucidated. Higher values of the Shannon index and Simpson index correspond to heightened biodiversity within the reactor. Upon comparing the Shannon index and Simpson index values obtained from samples within the same device at different time points, it becomes evident that the extension of membrane exposure time enhances the diversity and uniformity of microorganisms adhering to the hollow fiber membrane filaments in each device to varying degrees. Moreover, the Simpson index of the modified devices surpassed that of the unmodified reaction devices during the membrane formation period, signifying that the modified membrane surface facilitated efficient microbial attachment, culminating in a relatively stable and intricate community structure. On the 30th day, the Simpson index of the modified composite membrane based on PVDF notably exceeded that of the 2-4 reactor, indicating the effective enhancement of microbial affinity of the PVDF membrane grafted with acrylic acid. This enhancement aligns with the observed efficient NH_4^+ -N and TN removal rates in the 2-2 reactor.

Table 2. α Index of Diversity.

Sample ID	OTU	Chao	Coverage	Shannon	Simpon
1-1	904	1058	0.995060	4.85	0.015
1-2	1023	1190	0.994887	5.23	0.017
1-3	971	1044	0.996245	5.04	0.0114
1-4	815	1006	0.995282	4.67	0.0198
2-1	978	1180	0.993924	4.96	0.0187
2-2	1207	1409	0.993652	5.32	0.0221
2-3	1129	1276	0.994393	5.33	0.0122
2-4	821	997	0.995183	4.74	0.0201

3.3.2. Analysis of Microbial Community Structure

The changes in microbial community structure composition during the microbial biofilm formation period in each reactor at the phylum level are depicted in Figure 5a,b. The predominant microbial communities in each device primarily consisted of *Proteobacteria*, *Chloroflexi*, *Actinobacteria*, *Bacteroidetes*, and *Firmicutes*. Allegedly, the relative abundances of *Proteobacteria* and *Chloroflexi* are suggested to contribute to the degradation of organic pollutants [28–30]. As shown in Figure 5a, the proportion of *Proteobacteria* exhibited an increasing trend over time in R-PVDF, rising from 30.6% to 37.9%, and in R-PVDF-P-AA, increasing from 40.5% to 51.5%. This enhanced abundance within the modified PVDF membranes, compared to the original PVDF membranes at various time points, suggesting an improved capacity of PVDF-modified membranes to swiftly aggregate microorganisms and provide a conducive habitat for aerobic bacteria, thus enhancing the efficiency of NH_4^+ -N in wastewater [31–33]. *Chloroflexi*, representing denitrifying bacteria in wastewater treatment systems [34], may facilitate EPS production and provide a suitable environment for the bacteria [35]. Although the relative abundance of *Chloroflexi* in PVDF-based reactors decreased over time, their presence on PVDF membranes was more significant than that of the PTFE membranes.

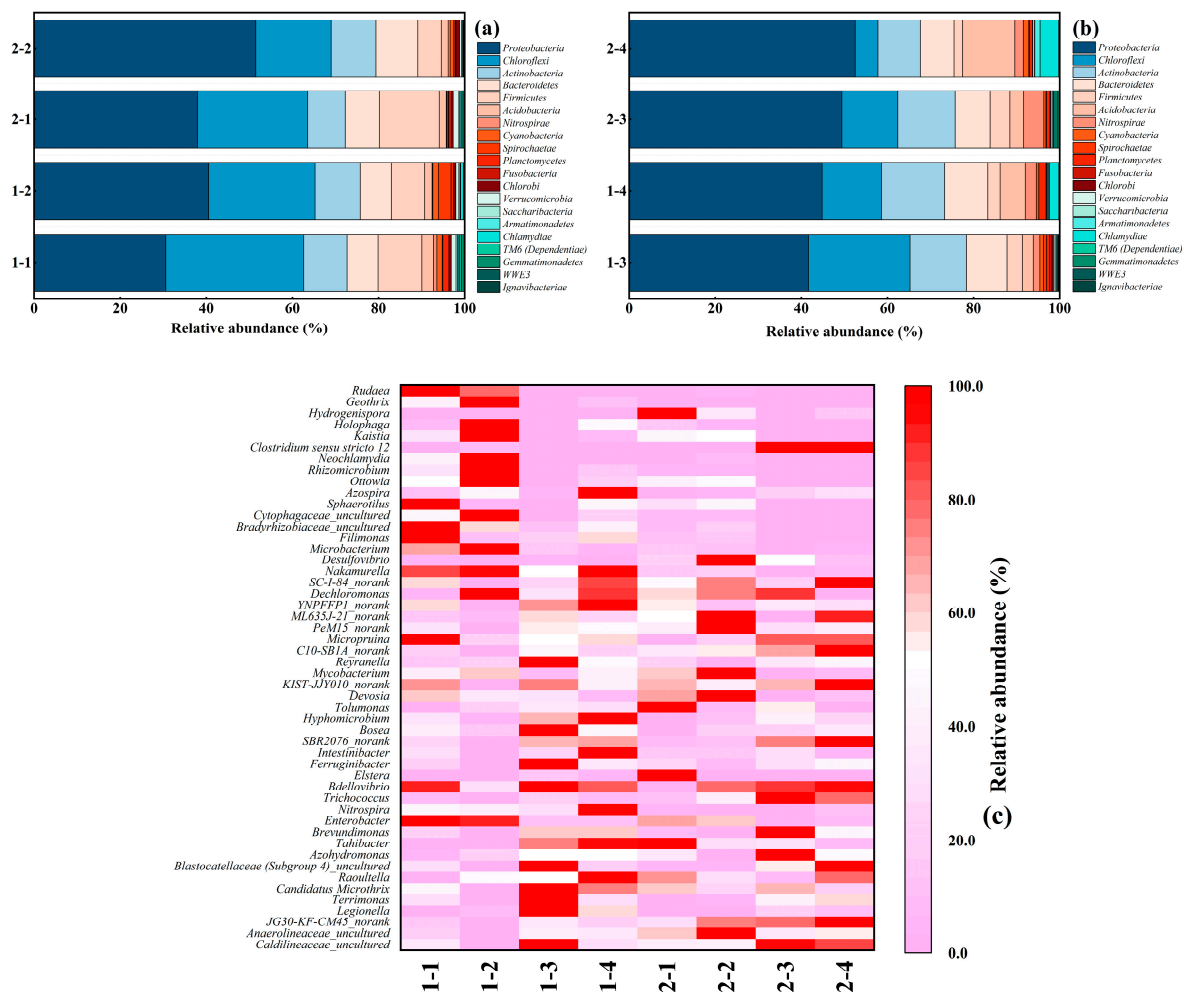


Figure 5. Column stacking charts showing changes of microbial communities at the phylum level for different samples: (a) microbial distribution and growth at 20 and 30 days in PVDF and PVDF-P-AA membranes; (b) microbial distribution and growth at 20 and 30 days in PTFE and PTFE-P-AA membranes. Heatmap (c) exhibits the relative abundance and distribution of the predominant species at the genus level.

The microbial affinity of PTFE-P-AA membranes was subtly enhanced compared to that of PTFE membranes. In the early period of membrane formation, a large number of *Proteobacteria* rapidly accumulated, becoming the dominant bacterial group and potentially improving the removal efficiency of $\text{NH}_4^+\text{-N}$ in wastewater. As the biofilm formation progressed, the relative abundance of *Proteobacteria* increased slightly in the two samples (from 44.8% to 52.5%), whereas that of *Chloroflexi* decreased (from 13.8% to 5.25%) in R-PTFE-P-AA—a situation. And the abundance *Chloroflexi* might cause $\text{NO}_3^- \text{-N}$ and $\text{NO}_2^- \text{-N}$ to pile up. On the 30th day, the modified PTFE membranes had a lower proportion of *Chloroflexi* (5.3%) compared to the original PTFE membranes (12.9%), which might not be conducive to the growth of denitrifying bacteria. Overall, this is consistent with the high TN removal rate observed in R-PVDF. Additionally, the abundance of *Firmicutes* in PVDF-based reactors (7.7% and 5.5%) was higher than in PTFE-based reactors (2.9% and 1.9%), reflecting their better ability to degrade complex and recalcitrant organic matter and endure extreme conditions [36–38]. Moreover, the proportion of *Nitrospirae* in reactor 2-3 (4.7%) was significantly higher than in the other reactors, indicating the potential to remove $\text{NH}_4^+\text{-N}$ later.

For a more comprehensive insight into the phylogenetic variance among the MABRs, we illustrate a heatmap depicting the microbial communities at the genus level in Figure 5c.

Notably, *Nakamurella*, a short rod-shaped, aerobic bacterium, plays a crucial role in stabilizing nitrogen removal and enhancing nitrite oxidation [39]. In this experiment, *Nakamurella* was significantly more abundant in reactors 1-2 and 1-4, comprising 16.5% and 15.8% of the microbial communities, respectively. *Nitrospira*, known for its role in nitrification [40,41], was more prevalent in reactor 1-4, constituting 8.1% of the microbial community. Moreover, *Devosia*, a genus within the class α -Proteobacteria of the phylum Proteobacteria, was also detected in reactor 1-4. However, the TN removal rates remained low, possibly due to the loss of denitrifying bacteria from the outer biofilm during sampling. *Trichococcus*, another dominant bacterium, can cause activated sludge swelling if its abundance exceeds 2%. Remarkably, reactors 2-3 and 2-4 exhibited *Trichococcus* levels of 9.32% and 7.23%, respectively, which may have significantly contributed to the poor NH_4^+ -N and TN removal rates observed. In the 2-2 reactor, the dominant presence of *Mycobacterium* and *Anaerolineaceae_uncultured*, both of which are capable of degrading organic matter and accelerating denitrification processes, contributed to the high TN removal rates. This indicates that the modified PVDF membrane was more effective in enriching denitrifying bacteria. Furthermore, the significant presence of uncultured *Caldilineaceae* in the R-PTFE reactor, a filamentous bacterium, can lead to bulking and foaming issues, thereby affecting the stability of biofilm formation [42,43]. This overgrowth may be associated with the low removal rates observed in R-PTFE.

3.3.3. Analysis of OTR after Operation of MABR

As the contact angle of the membrane decreases within a certain range, the area of contact between microorganisms suspended in wastewater and the membrane surface increases. This facilitates the attachment of microorganisms and a possible secretion of EPS, consequently leading to an increase in oxygen diffusion resistance [44]. Thus, we tested oxygen transfer performance after 30 days, as shown in Table 3. The OTR of PVDF-P-AA was $0.20 \text{ mg O}_2 \cdot \text{min}^{-1}$, and the reduction was only 9.09% compared to the 20.0% reduction of the pristine PVDF ($0.12 \text{ mg O}_2 \cdot \text{min}^{-1}$) membrane. Likewise, the modified PTFE membrane represented better oxygen transfer performance ($0.25 \text{ mg O}_2 \cdot \text{min}^{-1}$) compared to the original PTFE ($0.18 \text{ mg O}_2 \cdot \text{min}^{-1}$). Although the oxygen transfer capacity of the modified membrane was reduced to varying degrees during operation, it was still better than the original, showing a great potential for long-term operation.

Table 3. Oxygen transfer performance of diverse membranes.

Membrane Species	OTR-Before ($\text{mg O}_2 \cdot \text{min}^{-1}$)	OTR-After ($\text{mg O}_2 \cdot \text{min}^{-1}$)	Reduction
PVDF	0.15	0.12	20.0%
PVDF-P-AA	0.22	0.20	9.09%
PTFE	0.21	0.18	14.29%
PTFE-P-AA	0.26	0.25	3.8%

4. Conclusions

In summary, applying low-temperature plasma liquid-phase grafting of acrylic acid demonstrates the potential to enhance the hydrophilicity of hollow fiber membrane materials. Both types of modified hollow fiber membranes exhibit mildly improved degrees of improvement in micro-surface roughness, oxygen transport, and microbial affinity. In addition, after 30 days of operation, the modified membranes still maintained better oxygen transfer performance. Notably, the PVDF-modified membranes facilitated a rapid attachment of microorganisms in the initial stages of the reaction and the formation of stable biofilms, with the proportion of *Chloroflexi* bacteria present on PVDF membranes exceeding that found on the PTFE membranes. Regarding nitrogen removal of the PTFE-modified membrane, there are no apparent advantages compared with the original one. However, *Nitrospira* is the dominant genus gathered in the modified PTFE membrane. Consequently,

it is reasonable to assert that the PVDF membrane grafted with acrylic acid (PVDF-P-AA) via low-temperature plasma holds promise for potential applications in MABR systems.

Author Contributions: Methodology, X.L.; software, Q.Q.; data curation, Y.C.; writing—original draft preparation, W.Z. and Y.C.; writing—review and editing, W.Z. and D.L.; project administration, D.L.; funding acquisition, D.L. All authors have read and agreed to the published version of the manuscript.

Funding: This research was financially supported by the Key Research and Development Program of Zhejiang Province (No. 2022C02045) and the National Key R&D Program of China (No. 2022YFE0115600; 2022YFC3702004).

Data Availability Statement: The original contributions presented in the study are included in the article material, further inquiries can be directed to the corresponding author.

Acknowledgments: The authors sincerely thank the reviewers for their constructive comments to improve the manuscript.

Conflicts of Interest: The authors declare no conflicts of interest.

References

1. Li, Z.; Ren, L.; Qiao, Y.; Li, X.; Zheng, J.; Ma, J.; Wang, Z. Recent advances in membrane biofilm reactor for micropollutants removal: Fundamentals, performance and microbial communities. *Bioresour. Technol.* **2022**, *343*, 126139. [[CrossRef](#)] [[PubMed](#)]
2. Lu, D.; Bai, H.; Kong, F.; Liss, S.N.; Liao, B. Recent advances in membrane aerated biofilm reactors. *Crit. Rev. Environ. Sci. Technol.* **2021**, *51*, 649–703. [[CrossRef](#)]
3. Casey, E.; Glennon, B.; Hamer, G. Review of membrane aerated biofilm reactors. *Resour. Conserv. Recycl.* **1999**, *27*, 203–215. [[CrossRef](#)]
4. Semmens, M.J.; Dahm, K.; Shanahan, J.; Christianson, A. COD and nitrogen removal by biofilms growing on gas permeable membranes. *Water Res.* **2003**, *37*, 4343–4350. [[CrossRef](#)] [[PubMed](#)]
5. Klementiev, A.D.; Jin, Z.; Whiteley, M. Micron scale spatial measurement of the o₂ gradient surrounding a bacterial biofilm in real time. *mBio* **2020**, *11*, 1–7. [[CrossRef](#)] [[PubMed](#)]
6. Lackner, S.; Terada, A.; Horn, H.; Henze, M.; Smets, B.F. Nitrification performance in membrane-aerated biofilm reactors differs from conventional biofilm systems. *Water Res.* **2010**, *44*, 6073–6084. [[CrossRef](#)] [[PubMed](#)]
7. Ni, B.J.; Yuan, Z. A model-based assessment of nitric oxide and nitrous oxide production in membrane-aerated autotrophic nitrogen removal biofilm systems. *J. Membr. Sci.* **2013**, *428*, 163–171. [[CrossRef](#)]
8. Wu, Y.; Wu, Z.; Chu, H.; Li, J.; Ngo, H.H.; Guo, W.; Zhang, N.; Zhang, H. Comparison study on the performance of two different gas-permeable membranes used in a membrane-aerated biofilm reactor. *Sci. Total Environ.* **2019**, *658*, 1219–1227. [[CrossRef](#)]
9. McLamore, E.; Jackson, W.A.; Morse, A. Abiotic transport in a membrane aerated bioreactor. *J. Membr. Sci.* **2007**, *298*, 110–116. [[CrossRef](#)]
10. Syron, E.; Casey, E. Membrane-aerated biofilms for high rate biotreatment: Performance appraisal, engineering principles, scale-up, and development requirements. *Environ. Sci. Technol.* **2008**, *42*, 1833–1844. [[CrossRef](#)]
11. Martin, K.J.; Nerenberg, R. The membrane biofilm reactor (MBfR) for water and wastewater treatment: Principles, applications, and recent developments. *Bioresour. Technol.* **2012**, *122*, 83–94. [[CrossRef](#)]
12. Hou, F.; Li, B.; Xing, M.; Wang, Q.; Hu, L.; Wang, S. Surface modification of PVDF hollow fiber membrane and its application in membrane aerated biofilm reactor (MABR). *Bioresour. Technol.* **2013**, *140*, 1–9. [[CrossRef](#)]
13. Nisola, G.M.; Orata-Flor, J.; Oh, S. Partial nitrification in a membrane-aerated biofilm reactor with composite PEBA/PVDF hollow fibers. *Desalination Water Treat.* **2013**, *51*, 5275–5282. [[CrossRef](#)]
14. Cheng, C.-Y.; Chung, F.-Y.; Chou, P.-Y.; Huang, C. Surface Modification of Polytetrafluoroethylene by Atmospheric Pressure Plasma-Grafted Polymerization. *Plasma Chem. Plasma Process.* **2020**, *40*, 1507–1523. [[CrossRef](#)]
15. Wang, C.; Zhao, Y.; Ma, C.; Wang, X. Influence of mixed monomers on the microbial affinity properties of PTFE membranes modified by plasma methods. *Res. Environ. Sci.* **2020**, *33*, 465–470. [[CrossRef](#)]
16. Vatanpour, V.; Zoqi, N. Surface modification of commercial seawater reverse osmosis membranes by grafting of hydrophilic monomer blended with carboxylated multiwalled carbon nanotubes. *Appl. Surf. Sci.* **2017**, *396*, 1478–1489. [[CrossRef](#)]
17. Chen, K.-S.; Tsao, Y.-C.; Tsen, C.-H.; Chen, C.C.; Liao, S.-C. Cold Plasma Surface Modified Electrospun Microtube Array Membrane for Chitosan Immobilization and Their Properties. *World Acad. Sci. Eng. Technol. Int. J. Bioeng. Life Sci.* **2016**, *3*, 661–664.
18. Chen, W.-Y.; Matthews, A.; Jones, F.R.; Chen, K.-S. Deposition of a stable and high concentration of carboxylic acid functional groups onto a silicon surface via a tailored remote atmospheric pressure plasma process. *Surf. Coat. Technol.* **2018**, *336*, 67–71. [[CrossRef](#)]
19. Wang, J.; Nie, L.; Zhang, C.; Wang, B. Low-pressure air plasma-assisted acrylic grafted polyetherimide ultrafiltration membranes with excellent oil-water separation and high anti-fouling performances. *Mater. Today Commun.* **2023**, *35*, 106325. [[CrossRef](#)]
20. Khongnakorn, W.; Bootluck, W.; Jutaporn, P. Surface modification of FO membrane by plasma-grafting polymerization to minimize protein fouling. *J. Water Process Eng.* **2020**, *38*, 101633. [[CrossRef](#)]

21. Chen, Y.; Zhang, J.; Cohen, Y. Fouling resistant and performance tunable ultrafiltration membranes via surface graft polymerization induced by atmospheric pressure air plasma. *Sep. Purif. Technol.* **2022**, *286*, 120490. [[CrossRef](#)]
22. Characklis, W.G.; Wilderer, P.A. *The Structure and Function of Biofilms*; John Wiley & Sons: Chichester, UK, 1989.
23. Ganj, M.; Asadollahi, M.; Mousavi, S.A.; Bastani, D.; Aghaeifard, F. Surface modification of polysulfone ultrafiltration membranes by free radical graft polymerization of acrylic acid using response surface methodology. *J. Polym. Res.* **2019**, *26*, 231. [[CrossRef](#)]
24. Aksoy, Y.; Hasar, H. Fabrication of gas-permeable polyvinylidene fluoride (PVDF) hollow-fiber membrane by dry-jet wet spinning and its application in membrane biofilm reactors. *J. Water Process Eng.* **2021**, *40*, 101879. [[CrossRef](#)]
25. Zhao, Y.; Li, Y.; Yuan, S.; Zhu, J.; Houtmeyers, S.; Li, J.; Dewil, R.; Gao, C.; Van Der Bruggen, B. A chemically assembled anion exchange membrane surface for monovalent anion selectivity and fouling reduction. *J. Mater. Chem. A* **2019**, *7*, 6348–6356. [[CrossRef](#)]
26. Zhao, M.; Liu, Y.; Zhang, J.; Jiang, H.; Chen, R. Janus ceramic membranes with asymmetric wettability for high-efficient microbubble aeration. *J. Membr. Sci.* **2023**, *671*, 121418. [[CrossRef](#)]
27. Rana, D.; Matsuura, T. Surface modifications for antifouling membranes. *Chem. Rev.* **2010**, *110*, 2448–2471. [[CrossRef](#)] [[PubMed](#)]
28. Li, J.; Ma, J.; Liao, H.; Li, X.; Shen, L.; Lin, H.; Sun, L.; Ou, R.; He, D. Hot-pressed membrane assemblies enhancing the biofilm formation and nitrogen removal in a membrane-aerated biofilm reactor. *Sci. Total Environ.* **2022**, *833*, 155003. [[CrossRef](#)] [[PubMed](#)]
29. Sun, L.; Ma, J.; Li, L.; Tian, Y.; Zhang, Z.; Liao, H.; Li, J.; Tang, W.; He, D. Exploring the essential factors of performance improvement in sludge membrane bioreactor technology coupled with symbiotic algae. *Water Res.* **2020**, *181*, 115843. [[CrossRef](#)] [[PubMed](#)]
30. Ma, J.; Wang, Z.; Yang, Y.; Mei, X.; Wu, Z. Correlating microbial community structure and composition with aeration intensity in submerged membrane bioreactors by 454 high-throughput pyrosequencing. *Water Res.* **2013**, *47*, 859–869. [[CrossRef](#)]
31. Zhu, Y.; Wang, Y.; Jiang, X.; Zhou, S.; Wu, M.; Pan, M.; Chen, H. Microbial community compositional analysis for membrane bioreactor treating antibiotics containing wastewater. *Chem. Eng. J.* **2017**, *325*, 300–309. [[CrossRef](#)]
32. Choi, J.; Kim, E.S.; Ahn, Y. Microbial community analysis of bulk sludge/cake layers and biofouling-causing microbial consortia in a full-scale aerobic membrane bioreactor. *Bioresour. Technol.* **2017**, *227*, 133–141. [[CrossRef](#)] [[PubMed](#)]
33. Jo, S.J.; Kwon, H.; Jeong, S.Y.; Lee, C.H.; Kim, T.G. Comparison of microbial communities of activated sludge and membrane biofilm in 10 full-scale membrane bioreactors. *Water Res.* **2016**, *101*, 214–225. [[CrossRef](#)] [[PubMed](#)]
34. Lu, H.; Chandran, K.; Stensel, D. Microbial ecology of denitrification in biological wastewater treatment. *Water Res.* **2014**, *64*, 237–254. [[CrossRef](#)]
35. Gong, W.; Fan, A.; Zhang, H.; Luo, L.; Liang, H. Cow manure anaerobic fermentation effluent treatment by oxygen-based membrane aerated biofilm reactor. *Chem. Eng. J.* **2020**, *395*, 125116. [[CrossRef](#)]
36. Hu, Q.; Zhou, N.; Rene, E.R.; Wu, D.; Sun, D.; Qiu, B. Stimulation of anaerobic biofilm development in the presence of low concentrations of toxic aromatic pollutants. *Bioresour. Technol.* **2019**, *281*, 26–30. [[CrossRef](#)] [[PubMed](#)]
37. Zhao, L.; Su, C.; Liu, W.; Qin, R.; Tang, L.; Deng, X.; Wu, S.; Chen, M. Exposure to polyamide 66 microplastic leads to effects performance and microbial community structure of aerobic granular sludge. *Ecotoxicol. Environ. Saf.* **2020**, *190*, 110070. [[CrossRef](#)] [[PubMed](#)]
38. Lin, J.; He, H.; Zou, J.; Yang, Y.; Li, J. Effects of high-concentration influent suspended solids on aerobic granulation in sequencing batch reactors treating real textile wastewater. *J. Water Process Eng.* **2024**, *57*, 104609. [[CrossRef](#)]
39. Jiang, L.Q.; An, D.F.; Zhang, K.; Li, G.D.; Wang, X.Y.; Lang, L.; Jiang, M.G.; Wang, L.S.; Jiang, C.L.; Jiang, Y. *Nakamurella albus* sp. nov.: A Novel Actinobacterium Isolated from a Lichen Sample. *Curr. Microbiol.* **2020**, *77*, 1896–1901. [[CrossRef](#)]
40. Maixner, F.; Noguera, D.R.; Anneser, B.; Stoecker, K.; Wegl, G.; Wagner, M.; Daims, H. Nitrite concentration influences the population structure of Nitrospira-like bacteria. *Environ. Microbiol.* **2006**, *8*, 1487–1495. [[CrossRef](#)]
41. Harms, G.; Layton, A.C.; Dionisi, H.M.; Gregory, I.R.; Garrett, V.M.; Hawkins, S.A.; Robinson, K.G.; Sayler, G.S. Real-time PCR quantification of nitrifying bacteria in a municipal wastewater treatment plant. *Environ. Sci. Technol.* **2003**, *37*, 343–351. [[CrossRef](#)]
42. Guo, F.; Zhang, T. Profiling bulking and foaming bacteria in activated sludge by high throughput sequencing. *Water Res.* **2012**, *46*, 2772–2782. [[CrossRef](#)] [[PubMed](#)]
43. Meng, F.; Zhang, H.; Yang, F.; Li, Y.; Xiao, J.; Zhang, X. Effect of filamentous bacteria on membrane fouling in submerged membrane bioreactor. *J. Membr. Sci.* **2006**, *272*, 161–168. [[CrossRef](#)]
44. Wang, L.; Wu, Y.; Ren, Y.; Wang, Y.; Wang, Y.; Zhang, H. Transition of fouling characteristics after development of membrane wetting in membrane-aerated biofilm reactors (MABRs). *Chemosphere* **2022**, *299*, 134355. [[CrossRef](#)] [[PubMed](#)]

Disclaimer/Publisher's Note: The statements, opinions and data contained in all publications are solely those of the individual author(s) and contributor(s) and not of MDPI and/or the editor(s). MDPI and/or the editor(s) disclaim responsibility for any injury to people or property resulting from any ideas, methods, instructions or products referred to in the content.